



# Exact wave propagation analysis of lattice structures based on the dynamic stiffness method and the Wittrick–Williams algorithm

Xiang Liu <sup>a,b,c</sup>, Zhaoming Lu <sup>a,b,c</sup>, Sondipon Adhikari <sup>d</sup>, YingLi Li <sup>a,b,c,\*</sup>,  
J. Ranjan Banerjee <sup>e</sup>

<sup>a</sup> Key Laboratory of Traffic Safety on Track, Ministry of Education, School of Traffic & Transportation Engineering, Central South University, Changsha, China

<sup>b</sup> Joint International Research Laboratory of Key Technology for Rail Traffic Safety, Central South University, Changsha, China

<sup>c</sup> National & Local Joint Engineering Research Center of Safety Technology for Rail Vehicle, Central South University, Changsha, China

<sup>d</sup> James Watt School of Engineering, The University of Glasgow, Glasgow G12 8QQ, UK

<sup>e</sup> School of Mathematics, Computer Science and Engineering, City, University of London, London EC1V 0HB, UK

## ARTICLE INFO

Communicated by D. Yurchenko

### Keywords:

Wave propagation

Band gap

Dynamic stiffness method

Wittrick–Williams algorithm

Dispersion relations

## ABSTRACT

This paper proposes two significant developments of the Wittrick–Williams (W–W) algorithm for an exact wave propagation analysis of lattice structures based on analytical dynamic stiffness (DS) model for each unit cell of the structures. Based on Bloch's theorem, the combination of both the DS and the W–W algorithm makes the wave propagation analysis exact and efficient in contrast to existing methods such as the finite element method (FEM). Any number or order of natural frequencies can be computed within any desired accuracy from a very small-size DS matrix; and the W–W algorithm ensures that no natural frequency of the structure is missed in the computation. The proposed method is then applied to analyze the band gap characteristics and mode shapes of hexagonal honeycomb lattice structures and the results are validated and contrasted against the FE results. The effects of different primitive unit cell configurations on band diagrams and iso-frequency contours are thoroughly investigated. It is demonstrated that the proposed method gives exact eigenvalues and eigenmodes with the advantage of at least two orders of magnitude in computational efficiency over other methods. This research provides a powerful, reliable analysis and design tool for the wave propagations of lattice structures.

## 1. Introduction

Lattice structures can be constructed in the form of honeycomb structures obtained by tessellating unit cells in a certain predetermined shape [1], and each unit cell may comprise of a number of beam elements [2]. Common lattice structures include hexagonal and re-entrant [3–5], triangular [6,7], star-shaped [8,9], square and re-entrant [10,11], chiral lattices [12,13], and the one which is composed of two types of lattices [14,15] and there are several others.

Lattice structures have a number of distinguishing features and properties, such as good sound absorption, high strength or toughness, heat insulation, negative Poisson's ratio and flexible designability [16–21]. These attributes of lattice structures have inspired many investigations on wave propagation, especially on the dispersion relations such as the bandgap characteristics [22–24].

\* Corresponding author at: Key Laboratory of Traffic Safety on Track, Ministry of Education, School of Traffic & Transportation Engineering, Central South University, Changsha, China.

E-mail addresses: [xiangliu06@gmail.com](mailto:xiangliu06@gmail.com) (X. Liu), [1029975054@qq.com](mailto:1029975054@qq.com) (Z. Lu), [Sondipon.Adhikari@glasgow.ac.uk](mailto:Sondipon.Adhikari@glasgow.ac.uk) (S. Adhikari), [liyingsli@csu.edu.cn](mailto:liyingsli@csu.edu.cn) (Y. Li), [j.r.banerjee@city.ac.uk](mailto:j.r.banerjee@city.ac.uk) (J.R. Banerjee).

<https://doi.org/10.1016/j.ymssp.2022.109044>

Received 10 October 2021; Received in revised form 27 January 2022; Accepted 10 March 2022

0888-3270/© 2022 Elsevier Ltd. All rights reserved.

It is well-known that the frequency interval in which the wave motion cannot occur is called ‘bandgap’ or ‘stop band’. Interestingly, the earliest research on wave propagation in periodic structures can be traced back to Rayleigh [25] who first analyzed the wave propagation of periodic structure in 1887. Much later, Brillouin [26] proposed the theory of wave propagation in periodic structures in 1946. This was followed up by, Mead who [27] pointed out that the wave can pass through the periodic structure only within a specific frequency range and the wave propagation constant of an undamped periodic structure is essentially an eigenvalue problem [28,29].

The finite element method (FEM) is probably the most common numerical modeling method used for the wave propagation analysis of lattice structures. For example, Gonella and Ruzzene [30] established finite element models for unit cells of hexagonal and re-entrant lattices. By applying Bloch’s theorem, they converted the wave propagation analysis into a generalized eigenvalue problem with the natural frequencies being the eigenvalues. Martinsson and Movchan [31] derived dispersion equations for several two-dimensional lattice structures based on FE models and solved the transcendental equation numerically. Several modifications of the model were made by them to create complete band gaps at prescribed frequencies of the wave propagation problem. However, in their method, different dispersion equations were needed for different cells, making it rather tedious and less systematic. Casadei and Rimoli [32] used FEM to establish the models for unit cell of skew periodic lattice and they analyzed the effect of the geometrical parameters on anisotropy based on the Bloch’s theorem. The effect of the anisotropy on wave propagation was also investigated by them. Phani et al. [33] used finite element beam formulations and Bloch’s theorem to derive the dispersion equations for four representative planar lattice topologies and the influence of the beam slenderness ratio on the propagation of lattice waves was studied. Recently, Zhou et al. [34] applied the so-called numerical condensed wave finite element method to analyze the unit cell of two-dimensional lattice structures. In this method, the finite element formulation of the unit cell and the internal degrees of freedom are condensed based on matrix inversion. The complex wave-numbers are finally determined solving a polynomial eigenvalue problem. Nobrega et al. [35] applied the wave finite element method to investigate the bandgaps in periodic rods with periodically attached local resonators. Mencik and Duhamel [36] applied the wave finite element method to describe the dynamic behavior of periodic structures with arbitrary-shaped substructures connected along a straight direction. A symplectic transformation to improve the numerical stability in the computation of wave modes and model reduction techniques were applied to describe the dynamic behavior of the periodic structures in a specified direction. The literature shows that wave propagation can be widely investigated based on the above FE models. However, the conventional finite element method (CFEM) needs considerable mesh refinement during the modeling process to achieve sufficiently accurate results. This inevitably increases the computation time significantly, especially in the wave propagation analysis within the mid- to high-frequency ranges. To reduce the DoFs of the model, Chin et al. [37] proposed the spectral extended finite element method (X-FEM) where the shape functions used are high-order approximate polynomials. However, the formulation may lead to matrices that are not well-conditioned which may cause numerical singularities.

To avoid the above difficulties, researchers often apply analytical methods to model the unit cells. The transfer matrix method has been sometimes used to analyze 1D periodic structures. For instance, Chen and Wang [38] studied the wave propagation in periodic beams based on the transfer matrix method and Bloch’s theorem, and the relationship between the propagation constant and wave amplitudes was investigated by them. On the other hand, Yu et al. [11] applied the plane wave expansion method (PWEM) for the wave propagation analysis of membrane-like lattice structures and formulated the corresponding dispersion relations. Based on the PWEM and Bloch’s theorem, Miranda and Santos [10] investigated the complex band structure of the magnetoelastoelectric square lattice structure. Kutsenko et al. [39] applied the semi-analytical method (SAM) and Bloch’s theorem for the wave propagation analysis of two- and three-dimensional lattice structures. Leamy [40] presented an exact method for analyzing wave propagation in two-dimensional periodic structures, which combined the wave-based vibration analysis technique and Bloch’s theorem.

The dynamic stiffness method (DSM), or sometimes called the spectral element method (SEM) is another analytical modeling method which can use very few DoFs to represent the exact deformation of the structure in the entire frequency range [41–50]. The dynamic stiffness (or spectral element) formulation is essentially exact [51–53] which can generate the exact solution because the shape functions used are the exact solution of the governing differential equations instead of higher order approximate polynomials like the X-FEM [37]. Table 1 compares main differences among DSM, X-FEM and CFEM [54]. Moreover, DSM can also handle the complex structures comprising individual element DS matrices [55]. Based on the DSM (SEM), Zuo et al. [56] studied the wave propagation and response analysis of one-dimensional periodic truss structures. Wu et al. [57,58] used the dynamic stiffness (spectral element) model to analyze the wave propagation of one-dimensional periodic structures such as rod systems. They studied the vibration bandgap by establishing the spectral equation of the entire structure. The methods described above have also been applied to study the two and three-dimensional honeycomb lattices [59,60].

None the less, the determinant technique is normally used in the above methods to extract eigen-solutions from the analytical formulations, e.g., see [58,61]. Also, the solution process can sometimes be cumbersome, and inefficient, and more importantly, such methods likely to miss some natural frequencies. Therefore, it is necessary to apply an effective, reliable and accurate solution technique to compute eigen-solutions from analytical formulations.

It is well-known that Wittrick–Williams (W–W) algorithm [62] is an efficient, reliable and accurate eigen-solution technique, which ensures that no natural frequency of a vibrating structure is missed. Moreover, the Wittrick–Williams algorithm can pinpoint eigenvalues exactly (within any desired accuracy, even up to machine accuracy) by using, for example the bisection method [63,64]. As long as the formulation of the eigenvalue problem is exact, exact eigen-solutions can be achieved. Zhong et al. [65] first applied the W–W algorithm to analyze the wave propagation of chain-like periodic structures and obtained the band diagram. In these methods [65,66], the internal nodes of the structures were condensed by using a substructuring technique which made the formulation complex but made the computation more efficient. However, these studies on the application of Bloch’s theorem are

**Table 1**

Comparison of the dynamic stiffness method (DSM), the spectral extended finite element method (X-FEM) [37] and the conventional finite element method (CFEM) [54].  $\epsilon_1$  and  $\epsilon_2$  are the phase constants.

	DSM (present)	CFEM [54]	X-FEM [37]
Shape function	exact	low-order approximate polynomials	high-order approximate polynomials
Nos. of DoFs	small	large	medium
Nos. of accurate eigenvalue	infinite	$\ll DoFs$	$\le DoFs$
Accuracy in higher modes	exact	low accuracy	highly accuracy
Eigenvalue problem under Bloch boundary condition	single analytical DS matrix $K(\omega; \epsilon_1, \epsilon_2)$	separate numerical $K_n$ and $M_n$ matrices $K_n(\epsilon_1, \epsilon_2) - \omega^2 M_n(\epsilon_1, \epsilon_2)$	

generally confined to one-dimensional (chain-type) periodic structures [67,68]. By taking the analogy between structural mechanics and optimal control, the above methods were later improved by Zhong and Williams [66] by recasting the dynamic stiffness formulation into skew-symmetric matrices. The problem order was reduced by using a cell triangular decomposition and then the problem solved by the symplectic Householder transformation method. Hou et al. [69] developed a FE model for two-dimensional cellular structures and applied the symplectic analysis method for elastic wave propagation analysis. However, this method involves many sophisticated techniques such as the symplectic matrix algebra, the weighted adjoint symplectic orthonormality relationship, and the eigenvector expansion. All these complexities make the method inconvenient to use. Subsequently, the idea of the symplectic method was generalized to the continuous system and named as the structure-preserving method. This method also has been used to investigate the wave propagation problems in conservative system [70] and in non-conservative system [71–76]. In addition, Meng et al. [77] established the eigenvalue problem of hexagonal honeycomb lattice structures with cell walls of non-uniform thickness through finite element analysis and then they investigated the effect of the internal angle on the band gap characteristics. Side by side to the conventional finite element method [54], Hou and Meng used the substructure elimination method to simplify the FE matrix and they used W–W algorithm to obtain the eigenvalues indirectly. Although the W–W algorithm was applied in the above studies [69,77], the analysis was primarily based on the FE models which reduced the computation efficiency drastically, especially when more accurate results were required especially within mid- to high-frequency ranges.

Against this background, this paper proposes an exact, efficient and reliable analytical method to analyze the wave propagation in lattice structures. This new method combines the dynamic stiffness (DS) method [78] and the Wittrick–Williams (W–W) algorithm in an effective, efficient and exact way. The proposed method has the following advantages: (i) The shape functions of DSM used are essentially the exact general solutions of the governing differential equations, and therefore, the procedure leads to exact dynamic stiffness formulation; (ii) Only a few degrees of freedom are used to represent the wave propagation problem, leading to exact solutions with high computational efficiency; (iii) A small size dynamic stiffness matrix can be used to extract any number of eigenvalues without compromising the accuracy of the results. This is in sharp contrast to conventional FEM in which the number of eigenvalues depends on the dimensions of the stiffness and mass matrices; (iv) The usefulness of the dynamic stiffness method becomes apparent in solving the problem in the high frequency range; (v) The W–W algorithm ensures that no natural frequency is missed in the computation enabling computation of any required number of natural frequencies to any desired accuracy. The research described in this paper is especially relevant to wave propagation analysis in the high frequency range which is an essential requirement in the wave propagation control. The proposed method can be used to analyze the wave propagation problems for any lattice structure, including the production of the dispersion curves and surfaces.

The paper is organized as follows. After this Introduction section, Section 2 reviews the fundamentals of wave propagation in lattice structures and the dynamic stiffness formulation of unit cells. Section 3 proposes two enhanced versions of the W–W algorithm to extract eigenvalues and the mode shape computation algorithm. Section 4 demonstrates the efficiency and exactness of the proposed method using some carefully selected illustrative examples. Finally, Section 5 summarizes the paper.

## 2. Dynamic stiffness formulation for 2D lattice structures

Since a two-dimensional periodic lattice structure can be regarded as the primitive unit cell tessellated along a set of basis vectors  $(e_1, e_2)$  in direct lattice space, wave propagation in lattice structure can be investigated by using unit cell method based on Bloch’s theorem. In this section, the concept of Bloch’s theorem and the first Brillouin zone are introduced in Section 2.1, and the dynamic stiffness formulation for the unit cell is presented in Section 2.2.

### 2.1. Unit cell method of lattice structures based on Bloch’s theorem

According to the Bloch’s theorem, the wave motion of the lattice point  $j$ th in the  $(m, n)$  unit cell can be expressed as

$$q(\mathbf{r}) = q(\mathbf{r}_j) e^{k(\mathbf{r}-\mathbf{r}_j)} = q(\mathbf{r}_j) e^{(mk_1 + nk_2)} \tag{1}$$

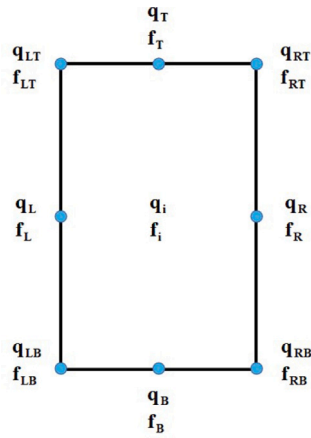


Fig. 1. Analysis of the degree of freedom of the general unit cell of periodic structure in two-dimensional space.

where  $q(\mathbf{r}_j)$  represents the displacement of the  $j$ th point of the primitive unit cell.  $k_i$  ( $i = 1, 2$ ) are the propagation constants [79] which can be written as  $k_i = \xi_i + i\varepsilon_i$ , where  $i = \sqrt{-1}$ ,  $\xi_i$  is the attenuation constant and  $\varepsilon_i$  is the phase constant [33]. It is generally considered that there is no attenuation during wave propagation, i.e.,  $\xi_i = 0$ .

2.1.1.1. Periodic boundary conditions based on Bloch’s theorem

A general unit cell with two-dimensional periodic structure is selected to illustrate the relationship between the lattice point displacement and force of two adjacent cells, as shown in Fig. 1. If the dynamic stiffness formulation for the unit cell is expressed as

$$\mathbf{K}(\omega)\mathbf{q} = \mathbf{f} \tag{2}$$

where  $\mathbf{K}(\omega)$  is the dynamic stiffness matrix,  $\mathbf{q}$  and  $\mathbf{f}$  are respectively the generalized displacement and the generalized force in the frequency domain. According to Bloch’s theorem of Eq. (1), the Bloch boundary condition related to the lattice points displacement are as follows

$$\mathbf{q}_R = e^{-i\varepsilon_1}\mathbf{q}_L, \mathbf{q}_T = e^{-i\varepsilon_2}\mathbf{q}_B, \mathbf{q}_{RB} = e^{-i\varepsilon_1}\mathbf{q}_{LB}, \mathbf{q}_{LT} = e^{-i\varepsilon_2}\mathbf{q}_{LB}, \mathbf{q}_{RT} = e^{-i(\varepsilon_1+\varepsilon_2)}\mathbf{q}_{LB} \tag{3}$$

Therefore, the generalized displacement  $\mathbf{q}$  can be simplified in the following form

$$\mathbf{q} = \mathbf{T}_B(\varepsilon_1, \varepsilon_2)\tilde{\mathbf{q}} \tag{4}$$

where  $\tilde{\mathbf{q}} = [\mathbf{q}_L \quad \mathbf{q}_B \quad \mathbf{q}_{LB} \quad \mathbf{q}_i]^T$ ,  $\mathbf{T}_B$  is the transformation matrix under the Bloch boundary conditions and expressed as

$$\mathbf{T}_B(\varepsilon_1, \varepsilon_2) = \begin{bmatrix} \mathbf{I} & 0 & 0 & 0 \\ \mathbf{I}e^{-i\varepsilon_1} & 0 & 0 & 0 \\ 0 & \mathbf{I} & 0 & 0 \\ 0 & \mathbf{I}e^{-i\varepsilon_2} & 0 & 0 \\ 0 & 0 & \mathbf{I} & 0 \\ 0 & 0 & \mathbf{I}e^{-i\varepsilon_1} & 0 \\ 0 & 0 & \mathbf{I}e^{-i\varepsilon_2} & 0 \\ 0 & 0 & \mathbf{I}e^{-i(\varepsilon_1+\varepsilon_2)} & 0 \\ 0 & 0 & 0 & \mathbf{I} \end{bmatrix} \tag{5}$$

Substituting Eq. (4) into Eq. (2), one has

$$\mathbf{K}(\omega)\mathbf{T}_B(\varepsilon_1, \varepsilon_2)\tilde{\mathbf{q}} = \mathbf{f} \tag{6}$$

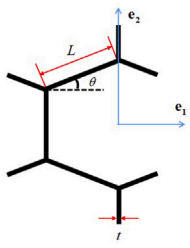
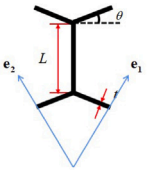
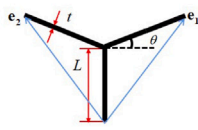
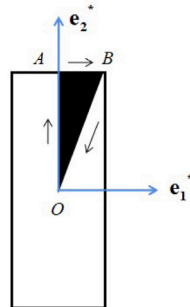
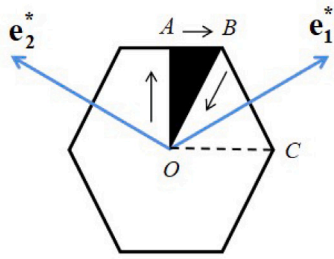
In order to satisfy force equilibrium, it is necessary to multiply the conjugate transpose of matrix  $\mathbf{T}_B$  on both sides of Eq. (6), leading to

$$\mathbf{T}_B^H(\varepsilon_1, \varepsilon_2)\mathbf{K}(\omega)\mathbf{T}_B(\varepsilon_1, \varepsilon_2)\tilde{\mathbf{q}} = \tilde{\mathbf{K}}(\omega; \varepsilon_1, \varepsilon_2)\tilde{\mathbf{q}} = \tilde{\mathbf{f}} \tag{7}$$

where  $\tilde{\mathbf{f}} = \mathbf{T}_B^H\mathbf{f}$ . For free wave propagation, the external force is considered to be zero (i.e.,  $\tilde{\mathbf{f}} = 0$ ).

The matrix  $\tilde{\mathbf{K}}(\omega; \varepsilon_1, \varepsilon_2)$  is the global dynamic stiffness matrix of the lattice structure dependent of three unknown elements, including the frequency  $\omega$ , phase constants  $\varepsilon_1$  and  $\varepsilon_2$ . An infinite number of natural frequencies can be obtained by varying  $\varepsilon_1$  and  $\varepsilon_2$  within the first Brillouin zone which is explained below.

**Table 2**  
Three typical primitive unit cell configurations of a hexagonal honeycomb structure and the corresponding direct lattice vector, reciprocal lattice vector, irreducible Brillouin zone and the high symmetric points.

	Model I	Model II	Model III
Primitive unit cell configurations			
Direct lattice vector	$e_1 = (L\cos\theta)\mathbf{i}$ $e_2 = \left(\frac{3L}{2}\right)\mathbf{j}$	$e_1 = (L\cos\theta)\mathbf{i} + (L + L\sin\theta)\mathbf{j}$ $e_2 = (-L\cos\theta)\mathbf{i} + (L + L\sin\theta)\mathbf{j}$	
Reciprocal lattice vector	$e_1^* = \left(\frac{2\pi}{L\cos\theta}\right)\mathbf{i}$ $e_2^* = \left(\frac{4\pi}{3L}\right)\mathbf{j}$	$e_1^* = \left(\frac{\pi}{L\cos\theta}\right)\mathbf{i} + \left(\frac{\pi}{L+L\sin\theta}\right)\mathbf{j}$ $e_2^* = \left(-\frac{\pi}{L\cos\theta}\right)\mathbf{i} + \left(\frac{\pi}{L+L\sin\theta}\right)\mathbf{j}$	
Irreducible Brillouin zone			
The high symmetric points	$O \quad (0, 0)$ $A \quad (0, \pi)$ $B \quad (\pi, \pi)$	$O \quad (0, 0)$ $A \quad 2\pi \left( \frac{1}{4\sin^2 I}, -\frac{1}{4\sin^2 I} \right)$ $B \quad 2\pi \left( 1 - \frac{1}{4\sin^2 I}, \frac{1}{4\sin^2 I} \right)$ $C \quad (\pi, \pi)$	

$$^1 I = \frac{\pi}{4} + \frac{\theta}{2}$$

<sup>2</sup>When  $\theta = 30^\circ$ , the irreducible Brillouin zone of Models II and III are the triangular OAB region.

### 2.1.2. The first Brillouin zone

In general, wave propagation analysis of periodic structures is performed along the boundary contour of the so-called first Brillouin zone [80]. However, the concept of the first Brillouin zone is introduced by reciprocal lattice. Given the basis vectors of the direct lattice, the reciprocal lattice can be obtained based on the following relation

$$\left. \begin{aligned} e_i \cdot e_j^* &= 2\pi & i &= j \\ e_i \cdot e_j^* &= 0 & i &\neq j \end{aligned} \right\} (i, j = 1, 2) \tag{8}$$

where  $e_j^*$  is the basis vector of the reciprocal lattice. The primitive unit cell of the reciprocal lattice is defined as the first Brillouin zone and it restricts the value of the wave vector. By limiting the phase constants to the contour of first Brillouin zone or the irreducible Brillouin zone, the behavior of the wave in the whole structure can be described.

In this paper, four lattice structures (hexagonal lattice, hexagonal re-entrant lattice, triangular lattice and Zigzag lattice) are considered. In general, the selection of the primitive unit cell for lattice structures is not unique and the corresponding first Brillouin zone is also different. In order to illustrate the unit cell method of the lattice structures based on Bloch's theorem, the hexagonal lattice structure is taken as an example. Three different kinds of representative primitive unit cells for hexagonal lattice structure and the corresponding direct lattice vectors, the reciprocal lattice vector, the irreducible Brillouin zone and the high symmetric points are illustrated in Table 2. It can be seen from Table 2 that Model I is based on the orthogonal basis whereas Model II and Model III are based on the non-orthogonal basis vector, which lead to the corresponding but distinguishing first Brillouin zones and high symmetric points. Finally, the bandgap properties can be computed by varying the phase constants in Eq. (7) along  $O - A - B - O$  or  $O - A - B - C - O$  contour of the corresponding first Brillouin zones respectively.

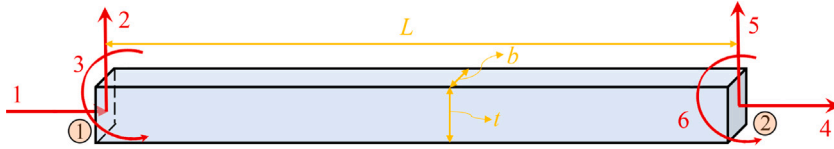


Fig. 2. A beam element with three degrees of freedom at each nodes. The degrees of freedom in each node correspond to the axial, transverse and rotational deformation.

### 2.2. Dynamic stiffness formulation for unit cell

Now we are in position to introduce the formulation of dynamic stiffness matrix  $K(\omega)$  of a unit cell in Eq. (2) based on the dynamic stiffness method. Upon selecting a suitable primitive unit cell, the corresponding dynamic stiffness formulation can be developed. The unit cell under consideration is composed of beams and each node of a beam has three degrees of freedom (DoFs) which takes into account the effects of axial, flexure and shear deformation as shown in Fig. 2. In this paper, the classical theory for axial vibration and the Timoshenko theory for bending vibration are applied to develop the DS formulation of the unit cell.

The governing differential equation in axial free vibration of a beam is

$$EA \frac{d^2U(x)}{dx^2} + \rho A \omega^2 U(x) = 0 \tag{9}$$

in which,  $EA$  is the stiffness for axial deformation,  $\rho A$  is mass per unit length and  $\omega$  is the circular frequency in  $rad/s$ . Based on the governing differential equation Eq. (9), the dynamic stiffness formulation for the axial vibration of the Timoshenko beam element [81] can be expressed as follows.

$$\begin{bmatrix} N_1 \\ N_2 \end{bmatrix} = \begin{bmatrix} a_1 & a_2 \\ a_2 & a_1 \end{bmatrix} \begin{bmatrix} U_1 \\ U_2 \end{bmatrix} \tag{10}$$

where

$$a_1 = E A k_a \cot(k_a L), a_2 = -E A k_a \csc(k_a L). \tag{11}$$

where  $L$  is the length of the beam and  $k_a^2 = \frac{\rho A \omega^2}{EA}$ .

The governing differential equations for free bending vibration based on the Timoshenko beam theory are given as follows

$$\begin{aligned} kAG \frac{d}{dx} \left( \frac{dW}{dx} - \theta \right) + \omega^2 \rho A W &= 0 \\ EI \frac{d^2\theta}{dx^2} + kAG \left( \frac{dW}{dx} - \theta \right) + \rho I \omega^2 \theta &= 0 \end{aligned} \tag{12}$$

where  $kAG$  and  $EI$  are the shear and bending stiffnesses of the beam,  $I$  is the second moment area of the beam cross section and  $\omega$  is the circular frequency in  $rad/s$ . Based on the governing differential equations Eq. (12), the dynamic stiffness matrix for the bending vibration of the Timoshenko beam element [82] can be written as follows.

$$\begin{bmatrix} V_1 \\ M_1 \\ V_2 \\ M_2 \end{bmatrix} = \begin{bmatrix} d_1 & d_2 & d_4 & d_5 \\ & d_3 & -d_5 & d_6 \\ & & d_1 & -d_2 \\ sym & & & d_3 \end{bmatrix} \begin{bmatrix} W_1 \\ \Theta_1 \\ W_2 \\ \Theta_2 \end{bmatrix} \tag{13}$$

where

$$\begin{aligned} d_1 &= R_3 \bar{b}^2 (\lambda_2 + \eta \lambda_1) (cS + \eta sC) / (\lambda_1 \lambda_2 \delta) \\ d_2 &= R_2 k_1 [(\lambda_1 + \eta \lambda_2) sS - (\lambda_2 - \eta \lambda_1) (1 - cC)] / \delta \\ d_3 &= R_1 (\lambda_2 + \eta \lambda_1) (sC - \eta cS) / \delta \\ d_4 &= -R_3 \bar{b}^2 (\lambda_2 + \eta \lambda_1) (S + \eta s) / (\lambda_1 \lambda_2 \delta) \\ d_5 &= R_2 k_1 (\lambda_2 + \eta \lambda_1) (C - c) / \delta \\ d_6 &= R_1 (\lambda_2 + \eta \lambda_1) (\eta S - s) / \delta \end{aligned} \tag{14}$$

with

$$\begin{aligned} R_j &= EI / L^j, \quad j = 1, 2, 3 \\ s &= \sin \lambda_1, \quad c = \cos \lambda_1, \quad S = \sinh \lambda_2, \quad C = \cosh \lambda_2 \\ \eta &= k_1 / k_2, \quad \delta = 2\eta(1 - cC) + (1 - \eta^2) sS \\ k_1 &= (\lambda_1^2 - \bar{b}^2 s^2) / \lambda_1, \quad k_2 = (\lambda_2^2 + \bar{b}^2 s^2) / \lambda_2 \end{aligned} \tag{15}$$

where

$$\left. \begin{matrix} \lambda_1 \\ \lambda_2 \end{matrix} \right\} = \bar{b} \left\{ \pm \Delta / 2 + [\Delta^2 / 4 + (1 - \bar{b}^2 r^2 s^2) / \bar{b}^2]^{1/2} \right\}^{1/2} \tag{16}$$

with

$$\Delta = r^2 + s^2, \quad \bar{b}^2 = \frac{\rho A \omega^2 L^4}{E}, \quad r^2 = \frac{I}{AL^2}, \quad s^2 = \frac{EI}{kAGL^2} \tag{17}$$

By integrating the axial vibration and bending vibration, the element DS matrix of a beam member can be written as

$$\mathbf{K}^e(\omega) = \begin{bmatrix} a_1 & 0 & 0 & a_2 & 0 & 0 \\ 0 & d_1 & d_2 & 0 & d_4 & d_5 \\ 0 & d_2 & d_3 & 0 & -d_5 & d_6 \\ a_2 & 0 & 0 & a_1 & 0 & 0 \\ 0 & d_4 & -d_5 & 0 & d_1 & -d_2 \\ 0 & d_5 & d_6 & 0 & -d_2 & d_3 \end{bmatrix} \tag{18}$$

and it needs to be transformed into global or datum coordinates. Subsequently, the global dynamic stiffness matrix of the unit cell  $\mathbf{K}(\omega)$  can be obtained by assembling the matrices of each beam member. The coordinate transformation procedure and the assembly procedure in the DSM are similar to that of the FEM [77]. Finally, the periodic boundary conditions will be applied to the dynamic stiffness matrix of the unit cell based on the Bloch’s theorem following the procedure described in Section 2.1.1.

### 3. The Wittrick–Williams algorithm for wave propagation analysis based on DS models

For the wave propagation analysis, the dispersion relations can be computed from the dynamic stiffness (DS) matrix of the unit cell of the lattice structure. Unlike the FEM, the natural frequencies cannot be suitably extracted directly from the DS matrix because the elements of the DS matrix are transcendental functions of the frequency. To address this issue, the Wittrick–Williams (W–W) algorithm [62] based on the Rayleigh theorem and Sturm sequence is exploited. By combining the Sturm sequence property with the bisection method, one can find the upper and lower bounds of the eigenvalues of a dynamic stiffness matrix, which makes the Wittrick–Williams algorithm robust and it ensures that no root is missed in the computation. The basic equation of the Wittrick–Williams algorithm can be expressed as

$$J(\omega^\#) = J_0(\omega^\#) + s \{ \mathbf{K}(\omega^\#) \} \tag{19}$$

where  $\omega^\#$  is the trial frequency,  $J_0$  count represents the number of natural frequencies below  $\omega^\#$  when the end nodes of the element are completely fixed.  $s \{ \mathbf{K}(\omega^\#) \}$  represents the number of negative diagonal elements after upper triangular transformation of  $\mathbf{K}(\omega)$  evaluated at  $\omega^\#$  when applying Gauss elimination to  $\mathbf{K}(\omega^\#)$ . The expression of  $J_0$  count can be written as

$$J_0(\omega^\#) = \sum_1^m J_i(\omega^\#) \tag{20}$$

where,  $J_i(\omega^\#)$  represents the number of natural frequencies lower than the trial frequency for the  $i$ th element when its end nodal displacements are zeros. It is necessary to obtain  $J_0$  count when using the Wittrick–Williams algorithm to ensure the certainly and high precision for the results especially analyzing vibration of complex structures at high frequency range. In view of this, we first summarize the  $J_i$  count for a beam member based on the classical theory and the Timoshenko theory which are given below.

For the classical theory(axial vibration):

$$J_i = \text{highest integer} < \frac{\phi_c}{\pi} \tag{21}$$

where  $\phi_c = \omega l \sqrt{\frac{\rho}{E}}$ .

For the Timoshenko theory(bending vibration):

$$J_i = j_c - \left[ 2 - \text{sgn}(d_3) - \text{sgn} \left( d_3 - \frac{d_6^2}{d_3} \right) \right] / 2 \tag{22}$$

where  $d_3, d_6$  are already given in Eq. (14) and  $j_c$  is given by:

$$\left. \begin{aligned} j_c &= j_d \quad \text{for } b^2 r^2 s^2 < 1 \\ j_c &= j_d + j_e \quad \text{for } b^2 r^2 s^2 \geq 1 \end{aligned} \right\} \tag{23}$$

with

$$\left. \begin{aligned} j_d &= \text{highest integer} < \frac{\lambda_1}{\pi} \\ j_e &= \text{highest integer} < \frac{\lambda_2}{\pi} + 1 \end{aligned} \right\} \tag{24}$$

where  $\lambda_1, \lambda_2$  have already been defined in Eq. (16).

Once  $J$  count of Eq. (19) is determined, the bisection method is generally used to pinpoint the natural frequencies for each order, and the natural frequency of the  $j$ th eigenvalue  $\omega_j$  can be determined within the frequency interval  $(\omega_{jl}^\#, \omega_{ju}^\#)$  where  $l$  and  $u$  indicate the lower and upper bound of the frequency. In order to achieve higher precision, the following criterion is set

$$\left| \omega_{ju}^\# - \omega_{jl}^\# \right| < \omega_{jl}^\# \times Tol. \tag{25}$$



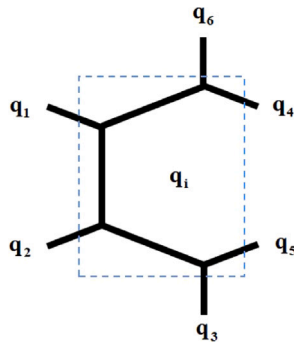


Fig. 3. Node displacements for Model I of hexagonal honeycomb lattice shown in Table 2:  $q_1 \sim q_6$  are the displacements of external nodes,  $q_i$  denotes the internal node displacements.

where  $Tol$  is the error tolerance required for the final result. The natural frequency of the  $j$ th order can then be expressed as

$$\omega_j = \frac{\omega_{ju}^\# + \omega_{jl}^\#}{2} (1 + Tol) \tag{26}$$

Indeed, the combination of dynamic stiffness method and the W–W algorithm greatly improves the efficiency of calculation and ensures the exactness of the results. This paper provides two enhancements of the W–W algorithms for computing the eigenvalues. Model I is used to illustrate the principles of these two developments in Sections 3.1 and 3.2 respectively. The procedures for mode shape computation are given in Section 3.3.

### 3.1. The Direct Wittrick–Williams algorithm

The Direct Wittrick–Williams (DWW) algorithm can be used to solve for the eigenvalues in a straightforward manner. In this work, the nodal displacements of Model I in Table 2 can be divided into internal nodal displacements  $q_i$  and external nodal displacements  $q_e = [q_1 \ q_2 \ q_3 \ q_4 \ q_5 \ q_6]^T$ , as shown in Fig. 3.

Based on the Bloch’s theorem and imposing the corresponding Bloch boundary conditions on the nodal displacements give

$$q_4 = e^{-i\varepsilon_1} q_1, q_5 = e^{-i\varepsilon_1} q_2, q_6 = e^{-i\varepsilon_2} q_3 \tag{27}$$

Using the above displacement relationships, the transformation matrix  $T_D$  and generalized displacement vector  $\tilde{q}_D$  can be obtained as

$$T_D(\varepsilon_1, \varepsilon_2) = \begin{bmatrix} \mathbf{I} & 0 & 0 & 0 & 0 \\ 0 & \mathbf{I} & 0 & 0 & 0 \\ 0 & 0 & \mathbf{I} & 0 & 0 \\ \mathbf{I}e^{-i\varepsilon_1} & 0 & 0 & 0 & 0 \\ 0 & \mathbf{I}e^{-i\varepsilon_1} & 0 & 0 & 0 \\ 0 & 0 & \mathbf{I}e^{-i\varepsilon_2} & 0 & 0 \\ 0 & 0 & 0 & 0 & \mathbf{I} \end{bmatrix} \tag{28}$$

$$\tilde{q}_D = [q_1 \ q_2 \ q_3 \ q_i]^T, q = T_D(\varepsilon_1, \varepsilon_2) \tilde{q}_D \tag{29}$$

After applying the Bloch boundary condition  $T_D$  upon the global DS matrix of the unit cell  $\mathbf{K}$ , we can arrive at the overall DS matrix of the unit cell to give

$$\mathbf{K}_D(\omega; \varepsilon_1, \varepsilon_2) = T_D^H(\varepsilon_1, \varepsilon_2) \mathbf{K}(\omega) T_D(\varepsilon_1, \varepsilon_2) \tag{30}$$

Then, the DWW algorithm can be used to calculate the natural frequency for free wave propagation problem, and the corresponding W–W algorithm equation can be written as

$$J(\omega^\#) = J_0(\omega^\#) + s \{ \mathbf{K}_D(\omega^\#) \} \tag{31}$$

### 3.2. Extended Wittrick–Williams algorithm

Compared with DWW algorithm, the extended Wittrick–Williams algorithm (EWW) requires the usual substructuring condensation method to condense the internal displacements in the eigenvalue computation.

For the free wave propagation, Eq. (2) can be written as

$$\mathbf{K}(\omega) q = \begin{bmatrix} \mathbf{K}_{ii} & \mathbf{K}_{ie} \\ \mathbf{K}_{ei} & \mathbf{K}_{ee} \end{bmatrix} \begin{bmatrix} q_i \\ q_e \end{bmatrix} = f = 0 \tag{32}$$



where,  $K_{ii}$ ,  $K_{ie}$ ,  $K_{ei}$  and  $K_{ee}$  are the block matrices of the dynamic stiffness matrix  $K$ . Using the usual substructuring condensation method, the external dynamic stiffness matrix  $\bar{K}$  can be expressed as

$$\bar{K}(\omega) = K_{ee} - K_{ei}K_{ii}^{-1}K_{ie} \tag{33}$$

Subsequently, the unit cell's equation of motion for free wave propagation related to the external component can be expressed as

$$\bar{K}(\omega) q_e = 0 \tag{34}$$

Using the displacement relationships in Eq. (27), we can formulate the transformation matrix  $T_E$  and generalized displacement vector  $\tilde{q}_E$  as

$$T_E(\epsilon_1, \epsilon_2) = \begin{bmatrix} I & 0 & 0 \\ 0 & I & 0 \\ 0 & 0 & I \\ Ie^{-i\epsilon_1} & 0 & 0 \\ 0 & Ie^{-i\epsilon_1} & 0 \\ 0 & 0 & Ie^{-i\epsilon_2} \end{bmatrix} \tag{35}$$

$$\tilde{q}_E = [q_1 \quad q_2 \quad q_3]^T, q_e = T_E(\epsilon_1, \epsilon_2) \tilde{q}_E \tag{36}$$

After applying the Bloch boundary conditions  $T_E$  upon the global DS matrix of the unit cell  $K$ , we can arrive at the overall DS matrix of the unit cell as

$$K_E(\omega; \epsilon_1, \epsilon_2) = T_E^H(\epsilon_1, \epsilon_2) \bar{K}(\omega) T_E(\epsilon_1, \epsilon_2) \tag{37}$$

Once the dynamic stiffness matrix  $K_E$  of the unit cell is obtained, the EWW algorithm can be used to calculate the natural frequencies. In order to compensate for the condensation of the internal displacements, an extra term  $s\{K_{ii}\}$  is necessary to be considered. Therefore, the basic equation of EWW algorithm can be written as

$$J(\omega^\#) = J_0(\omega^\#) + s\{K_E(\omega^\#)\} + s\{K_{ii}(\omega^\#)\} \tag{38}$$

### 3.3. Mode shape computation

Once the natural frequency at a certain combination of wave numbers is obtained, we can compute the corresponding eigenvector (displacement vector) to determine the modes of the unit cell of the lattice structure. The procedures for the modal shape computation method based on DSM-DWW are given as follows.

- (i) Find the corresponding row  $h$  of the smallest diagonal element in the diagonal matrix triangulated from the dynamic stiffness matrix  $K_D^A$ ;
- (ii) Set the corresponding element in displacement vector as 1, and then calculate the values of other elements in terms of the chosen displacement to obtain the generalized displacement vector  $\tilde{q}_D$  under the simplified Bloch coordinates;
- (iii) Use Eq. (4) to compute the global generalized displacement vector for the unit cell;
- (iv) Transform the global generalized displacement  $q$  from global to local coordinate through  $q_l = Tq$ , where  $q_l$  is the global generalized displacement at local coordinate;
- (v) Substitute  $q_l$  into the shape functions [81,82] to recovery the mode shape.

The process for the modal shape computation method based on DSM-EWW is similar to the one whose based on DSM-DWW, and the difference is that we cannot obtain the global generalized displacement vector directly as in the case with DWW. The specific steps for the EWW case are given below.

- (i) Find the row  $h$  of the smallest element of the diagonal of dynamic stiffness matrix  $K_E^A$ ;
- (ii) Let the corresponding element in displacement vector  $\tilde{q}_E$  as 1, and then calculate the values;
- (iii) Use Eq. (36) to compute the external generalized displacement vector  $q_e$  for the unit cell;
- (iv) Compute the elements of the inner generalized displacement vector by Eq. (32) and formulate the global generalized displacement vector;
- (v) The global generalized displacement vector  $q_l$  in local coordinate can be obtained from  $T \times q$ ;
- (vi) Substitute  $q_l$  into the shape functions [81,82] to recovery the mode shape.

By comparing two versions of the modal shape computation method, it is obvious that the modal shape computation based on DSM-DWW is more efficient than DSM-EWW because the dynamic stiffness matrix  $K_D$  is direct. Therefore, the DSM-DWW method is chosen to compute the mode shape of the lattice structures in this paper.

## 4. Results and discussions

In this section, the proposed method is applied to analyze the wave propagation properties of the lattice structures. First, in order to highlight the reliability of the proposed method, Section 4.1 compares the proposed efficient method with other method in term of the results and the computational efficiency. Section 4.2 investigates the effect of the primitive unit cell configurations on the dispersion relations. Section 4.3 uses the proposed mode shape computation algorithm to investigate the mode shapes of the hexagonal lattice.

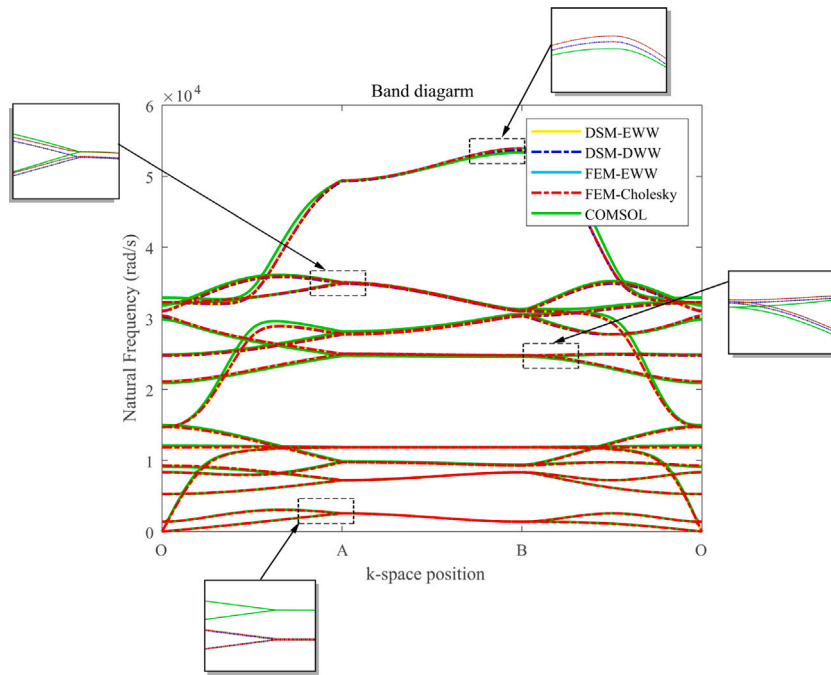


Fig. 4. The first fifteen dispersion curves calculated by DSM-DWW, DSM-EWW, FEM-EWW, FEM-Cholesky and COMSOL.

#### 4.1. Validation and comparison of different computation algorithms

To verify the efficiency and reliability of the proposed method, a comparative study is performed based on the dispersion relations of the hexagonal lattice structure. The primitive unit cell selected in this subsection is Model I. The unit cell is modeled by Timoshenko beams with length  $L = 0.1$  m and rectangular cross-section (height  $h = 0.001$  m, width  $t = 0.002\sqrt{3}$  m). The unit cell angle  $\theta = 30^\circ$  and the material parameters include Young's modulus  $E = 72$  GPa, density  $\rho = 2700$  kg/m<sup>3</sup>, and Poisson's ratio  $\mu = 0.3$ . Five methods are used in the analysis. These are dynamic stiffness method combined with the direct Wittrick–Williams (DWW) algorithm (DSM-DWW), dynamic stiffness method combined with extended Wittrick–Williams (EWW) algorithm (DSM-EWW), finite element method combined with the extended Wittrick–Williams algorithm (FEM-EWW), finite element method combined with Cholesky algorithm (FEM-Cholesky), commercial software COMSOL, respectively. The results are performed on the same computer which the CPU and RAM is 3.00 GHz and 8.00 GB respectively, and the band diagrams are presented in Fig. 4.

Fig. 4 essentially shows that the band diagrams obtained from the DSM-DWW and DSM-EWW analysis are completely coincide, meanwhile, the band diagrams obtained from the FEM-EWW and FEM-Cholesky analysis match exactly with each other (Note that the results of DSM-EWW, DSM-DWW, FEM-EWW and FEM-Cholesky are based on the same beam theory). Also, it is clear that the FEM results (FEM-EWW and FEM-Cholesky) are always larger than the DSM results (DSM-EWW, DSM-DWW) when the model modeled by beam elements, this is expected due to the discretization errors involved in the FEM analysis. Furthermore, some parts of the curves calculated by COMSOL are above the DSM results while others are below. This might be because the finite element solid model is used in COMSOL analysis so that the discrepancies are caused by the joint influences of both the FE discretization errors and the differences between solid and beam models.

Within the first one hundred order of natural frequencies for point B in Fig. 4, some selected frequencies computed by the above five methods are compared in Table 3. By comparing the results computed by using the dynamic stiffness (DS) model and the finite element (FE) model, it can be concluded that the convergence state is not reached when the FE model is meshed into 138 DoFs and the results converge when the FE model is meshed into 813 DoFs, which also can be summarized as FEM results converge toward DSM results. Furthermore, it can be seen that the COMSOL results are similar to DSM results (DSM-DWW, DSM-EWW) as the solid model is meshed into 15094 DoFs. The relative errors of FEM results (with coarse and fine meshes) and COMSOL results (with coarse and fine meshes) with respect to the results computed by the proposed DS model for some representative eigenvalues are shown in Fig. 5. It can be seen that for higher-order eigenvalues ( $\omega_{30}$ ,  $\omega_{50}$ ), the relative errors of FEM and COMSOL results based on coarse meshes with respect to the DSM results are significantly large, but those with finer meshes with a large number of DoFs (with 813 and 15094 DoFs respectively) match very well with the DSM results.

For efficiency, the DSM-WW is at least three orders of magnitude higher than the FEM-EWW [9] when the results satisfy the accuracy requirements, especially the DSM-EWW which only takes 6.88 s while the FEM-EWW takes as long as 110020.55 s. Meanwhile, the FEM-Cholesky method takes as long as 190.31 s to compute the natural frequencies while the proposed DSM-EWW takes only 6.88 s. Moreover, it can be ascertained from Table 3 that the efficiency for DSM-EWW is about 4 times higher than

**Table 3**

Natural frequencies in *rad/s* and computational time (Comp. Time) of the band diagram on Point B of Fig. 4 by using five different methods, namely, (i) DSM-DWW; (ii) DSM-EWW; (iii) FEM-Choleshy; (iv) FEM-EWW; (v) COMSOL software. Different numbers of degrees of freedom (DoFs) are adopted for different methods, in which ‘in’ means the number of internal DoFs whereas ‘ex’ means the number of external DoFs. ‘\’ means the natural frequency or the computational time cannot be calculated.

Model	DSM		FEM-EWW [9]		FEM		COMSOL	
	DWW	EWW	120(in)+18(ex)	795(in)+18(ex)	138	813	466	15094
Solu.tech.					Choleshy			
DOFs	30	12(in)+18(ex)	120(in)+18(ex)	795(in)+18(ex)	138	813	466	15094
$\omega_1$	1378.25	1378.25	1387.80	1378.37	1387.80	1378.37	1414.99	1389.63
$\omega_2$	1378.25	1378.25	1390.18	1378.43	1390.18	1378.43	1415.24	1389.63
$\omega_3$	8334.97	8334.97	8642.21	8340.78	8642.21	8340.78	8784.91	8317.76
$\omega_4$	8334.97	8334.97	8822.67	8345.59	8822.67	8345.59	8821.92	8317.76
$\omega_5$	9280.71	9280.71	9812.92	9285.58	9812.92	9285.58	10223.28	9403.32
$\omega_{10}$	24729.32	24729.32	29296.79	24833.01	29296.79	24833.01	30129.77	24588.21
$\omega_{20}$	59168.27	59168.27	85728.42	59325.73	85728.42	59325.73	72624.64	60464.07
$\omega_{30}$	107050.32	107050.32	186067.67	108887.49	186067.67	108887.49	179854.84	107593.93
$\omega_{40}$	195340.45	195340.45	305568.46	198808.41	305568.46	198808.41	286071.54	193972.32
$\omega_{50}$	254960.84	254960.84	465582.85	258627.26	465582.85	258627.26	448948.07	264102.41
$\omega_{100}$	712508.71	712508.71	\	740697.06	\	740697.06	1553852.85	718221.93
Comp.time (s)	24.75 s	6.88 s	\	11002.55 s	\	190.31 s	54 s	467 s

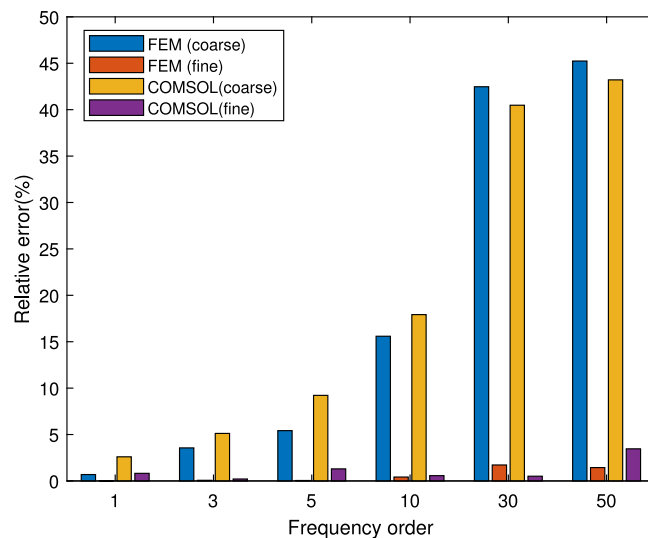


**Fig. 5.** The relative error between the results by the FEM with a coarse mesh (138 DOFs) and a fine mesh (813 DOFs) and those by COMSOL with a coarse mesh (466 DOFs) and a fine mesh (15094 DOFs) compared to the DSM results given in Table 3.

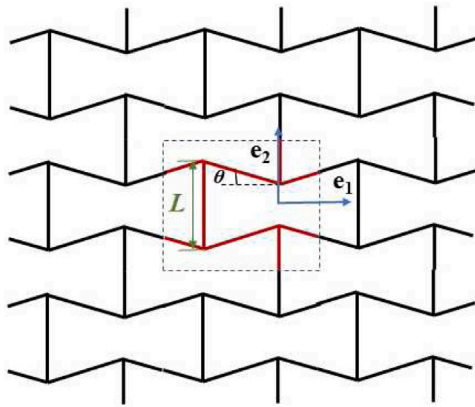
**Table 4**

Comparison of the two types of the Wittrick–Williams algorithms based on dynamic stiffness method.

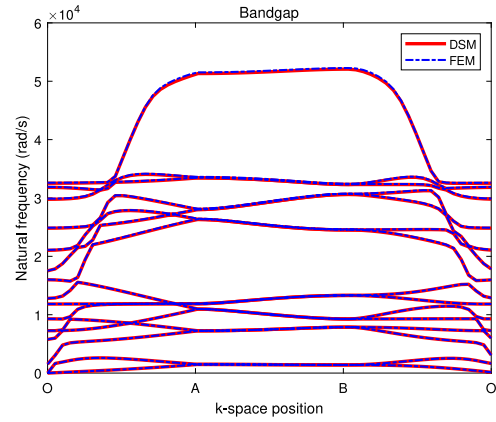
	DSM-DWW	DSM-EWW
Model difficulty	Low	Comparatively low
Numerical stability	Stable(no matrix inversion)	Less stable (matrix inversion)
Efficiency	Efficient	Highly efficient
Mode shape computation	Reliable for local modes	Less reliable for local modes

DSM-DWW, which is the consequence of using the usual substructuring condensation method to reduce the size of the dynamic stiffness matrix. The comparison of DSM-DWW and DSM-EWW is shown in Table 4.

In order to demonstrate the wide application scope, the proposed method is also applied for the wave propagation analysis of other three types of lattice structures, namely, hexagonal re-entrant lattice, triangular lattice and Zigzag lattice, see Figs. 6 to 8. The dimensional parameters and material parameters of each beam element are the same as those used in the hexagonal lattice structure previously in Table 3 and Fig. 4. The corresponding primitive unit cells are shown in red, and the band diagrams computed by the proposed method are compared with FEM results with fine meshes (each beam member is modeled by 30 FE elements), which shows great consistency.

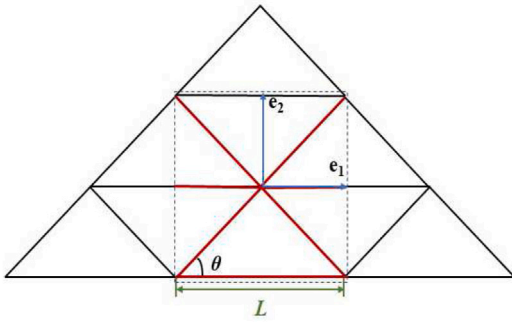


(a) Primitive unit cell

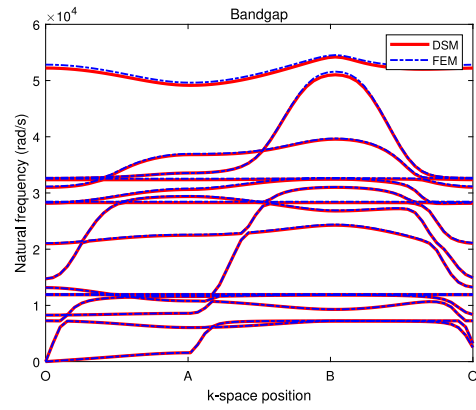


(b) Band diagram

Fig. 6. The primitive unit cell of hexagonal re-entrant lattice and the band diagram with the unit cell angle  $\theta = 10^\circ$ .

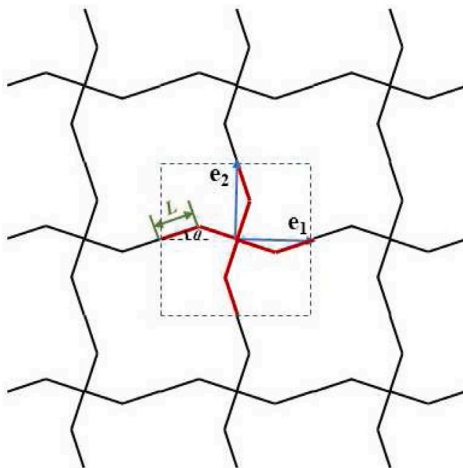


(a) Primitive unit cell

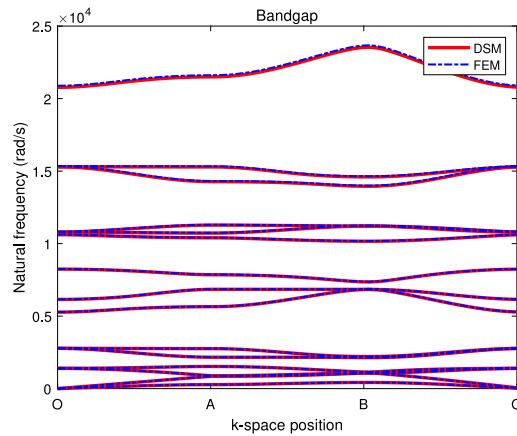


(b) Band diagram

Fig. 7. The primitive unit cell of triangular lattice and the band diagram with the unit cell angle  $\theta = 60^\circ$ .



(a) Primitive unit cell

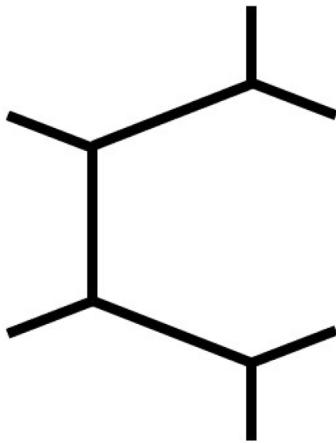


(b) Band diagram

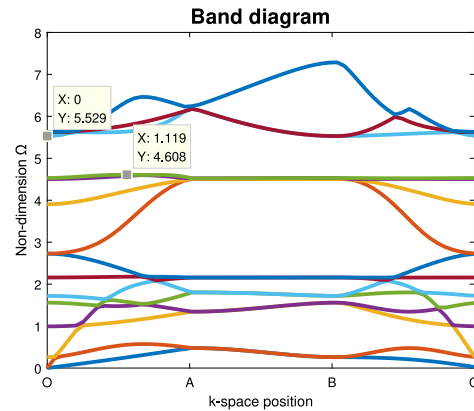
Fig. 8. The primitive unit cell of Zigzag lattice and the band diagram with the unit cell angle  $\theta = 60^\circ$ .

**Table 5**  
Comparison of the computation time, the bandgap position, and bandgap size of the first fifteen dispersion curves by using the Bloch wave analysis on different primitive unit cells of the hexagonal lattice structure.

Hexagonal honeycomb lattice				
Primitive unit cell	DSM-EWW	DSM-DWW	Bandgap position	Bandgap size
Model I	7.4 s	26.3 s	12th–13th	4.608–5.529
Model II	5.3 s	7.2 s	6th–7th	4.608–5.529
Model III	3.4 s	3.4 s	6th–7th	4.608–5.529



(a) Configuration of Model I



(b) Band diagram

Fig. 9. The first fifteen dispersion curves obtain by using the Bloch wave analysis on Model I.

4.2. The effect of the primitive unit cell configurations on dispersion relations

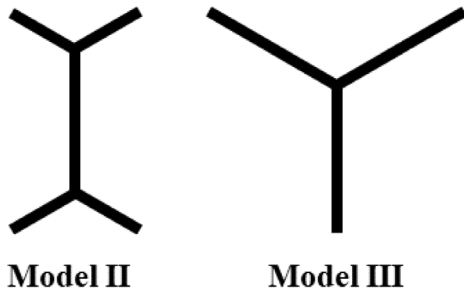
In this subsection, the effect of the primitive unit cell configurations of the hexagonal lattice structure on the band diagrams and Iso-frequency contours are investigated. The primitive unit cells are shown in Table 2 and modeled by Timoshenko beams with length  $L = 0.1$  m and rectangular cross-section (height  $h = 0.001$  m, width  $t = 0.004\sqrt{3}$ m). The unit cell angle  $\theta = 30^\circ$  and the material parameters include Young’s modulus  $E = 72$  GPa, density  $\rho = 2700$  kg/m<sup>3</sup>, and Poisson’s ratio  $\mu = 0.3$ . The first fifteen branches of dispersion curves are considered and the results are made dimensionless using the following expressions

$$\omega_0 = \frac{\pi^2}{La^2} \sqrt{\frac{EI_z}{\rho A}}, \Omega = \frac{\omega}{\omega_0} \tag{39}$$

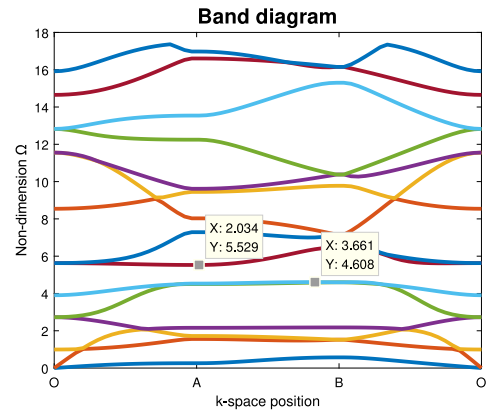
where  $A$  and  $I_z$  are the cross-sectional area and the axial moment of inertia of the Timoshenko beam respectively.

The corresponding computation time, band gap position and the band gap size are shown in Table 5. Obviously, it can be seen that the simpler primitive unit cell configuration leads to the higher computational efficiency. At the same time, it can be noticed that the superiority of DSM-EWW algorithm is evident when the primitive unit cell is more complex. The band diagram obtained by using the Bloch wave analysis for Model I is shown in Fig. 9(b). It can be seen that there exists a complete bandgap between the 12th branch and 13th branch, which does not occur in the case of the slenderness ratio of 100. The above procedure is applied to analyze Model II and Model III of Table 2. It is interesting that the corresponding band diagrams are the same. This is because the two models based on the same basis vectors. The corresponding band diagrams are shown in Fig. 10(b). A complete bandgap can be detected between the 6th branch and 7th branch. Comparing the above band diagrams, it is clear that both the bandgaps occur in the non-dimensional frequency range [4.687–5.529]. It can be concluded that for any lattice structure, the bandgap will not change due to the differences in the primitive unit cell configurations. In addition, the dispersion relations generated by analyzing the primitive unit cell which is based on the same basic vectors show no difference at all.

The iso-frequency contour is another important form to describe the dispersion relations. The effects of the primitive unit cell configurations on the iso-frequency are studied by using the Bloch wave analysis and the corresponding iso-frequency contours are given in Figs. 11 and 12. The first eight surfaces in Fig. 12 are similar to those in [83], and the small difference is due to the additional mass added to the lattice points in [83]. Meanwhile, there is a sharp contrast between Figs. 11 and 12 that Model I leads to iso-frequency contours being symmetric to an axis parallel to  $x$  and  $y$  axis while the iso-frequency contours of Model II and Model III have the symmetry with respect to the diagonal axis. The above contrast stems from the basis vectors are different and it has no effect on investigating the behaviors of the hexagonal lattice structure. For example, the comparison between Figs. 11(a) and 12(a) both shows that the isotropic characteristic is presented in the low-frequency range. The curves change rapidly in the



(a) Configurations of Models II and III



(b) Band diagram

Fig. 10. The first fifteen dispersion curves obtain by using the Bloch wave analysis on Models II or III.

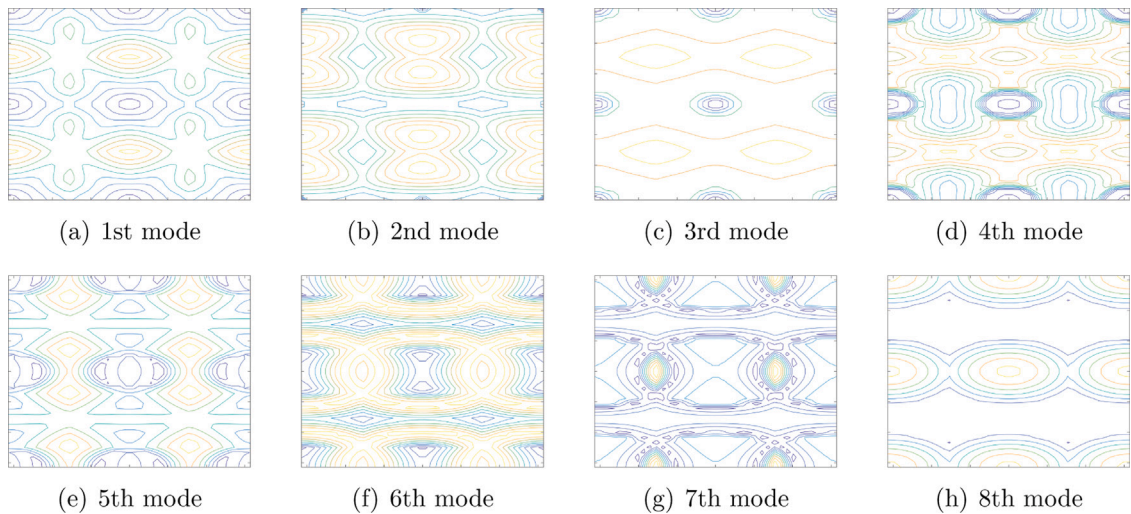


Fig. 11. The first eight iso-frequency contours obtain by using the Bloch wave analysis on Model I.

high-frequency range of the vertical direction for Fig. 11(e) and the corresponding behavior occurs in directions inclined at 135° for Fig. 12(e), which can be explained by the relevant basis vectors.

### 4.3. Modal shape analysis

It is well recognized that mode shape describes wave propagation in lattice structures. Each point on the dispersion curve represents the eigenvalue under a certain wavenumber. After the eigenvalues are calculated, the modal shape computation method which is based on DSM-DWW can be used to compute the local displacement for each node (Local mode). Model II is selected to analyze due to the required lattice points are included. Considering the wave passes through the lattice structure along the vertical direction (OA direction). We choose three states of the wave number on that direction to analyze, which are  $k_1 = 0, k_2 = 0$  (point O);  $k_1 = \frac{\pi}{2}, k_2 = \frac{\pi}{2}; k_1 = \pi, k_2 = \pi$  (point A).

The first five mode shapes of each state are shown in Table 6, and they are compared with COMSOL’s result. Combining the above results with the band diagram of Fig. 10(b) for discussion, it can be concluded that the first two branches at point O are close to zero which leads the corresponding modes being the rigid body modes. It may be noticed that as the frequencies increase gradually in the OA direction for the second branch and the fifth branch of the dispersion curves, and the corresponding mode shapes transform from simple to complex.



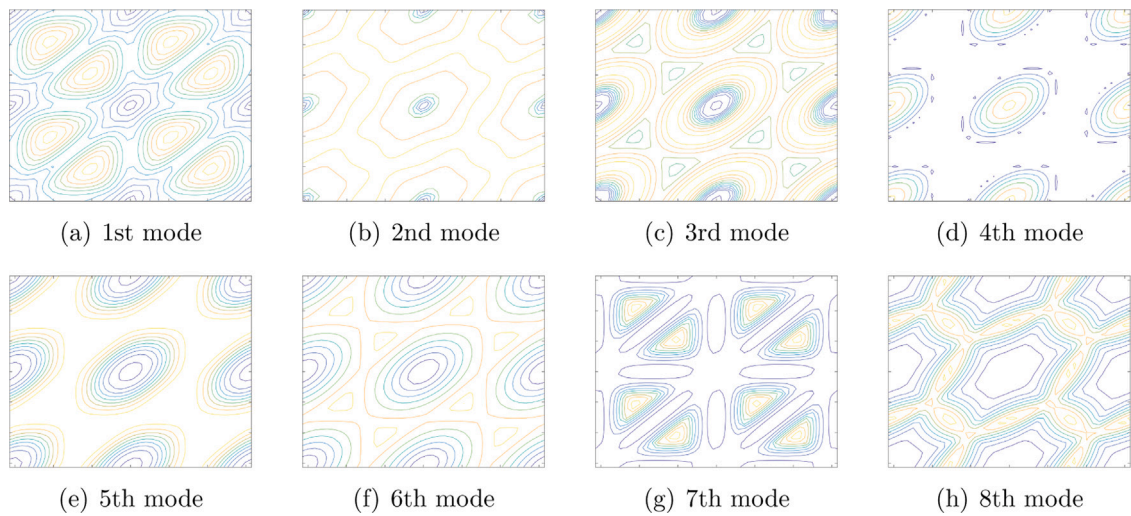


Fig. 12. The first eight iso-frequency contours obtain by using the Bloch wave analysis on Model II or Model III.

**Table 6**  
The first five modes of the hexagonal lattice in three wavenumeral states for the vertical direction (OA direction).

Mode	DSM	COMSOL	DSM	COMSOL	DSM	COMSOL
	$k_1 = 0, k_2 = 0$		$k_1 = \frac{\pi}{2}, k_2 = \frac{\pi}{2}$		$k_1 = \pi, k_2 = \pi$	
1						
2						
3						
4						
5						

### 5. Conclusions

The contributions made in this paper are as follows. First, based on Bloch’s theorem, two versions of the Wittrick–Williams algorithm based on dynamic stiffness models for analyzing the wave propagation of lattice structures are proposed which reduce the computational load dramatically and can obtain the exact solutions. Secondly, two types of modal shape computation method are developed based on the new proposed methodologies. Next, the proposed methodologies are applied to investigate the effect of the primitive unit cell configurations on dispersion relations, such as the band diagrams and the corresponding iso-frequency contours.

Three kinds of the primitive unit cell configurations based on the dynamic stiffness method and Bloch wave analysis of the hexagonal honeycomb lattice structure have been given, namely, Model I, Model II and Model III. Using the Bloch wave analysis on Model I, the reliability of the proposed methodologies has been verified by comparing the band diagrams obtained by the proposed methods with FEM-EWW, FEM-Cholesky and COMSOL. It is observed that the proposed methods can ensure the exactness of the results by using only a few DoFs, especially in mid-to high-frequency ranges. Moreover, the computational efficiency is more than two orders of magnitude higher than other methods such as FEM.



Comparison of the computational time for dispersion curves obtained by using the Bloch wave analysis on the above three kinds of the primitive unit cells shows the combination of the extended Wittrick–Williams algorithm and dynamic stiffness model has much higher efficiency, especially when considering the complex primitive unit cell. The dispersion relations may differ due to changes in the primitive unit cell configuration but the corresponding bandgaps are occurred in the same frequency interval. The mode shapes of the hexagonal lattice structure have been studied by using the proposed modal shape computation method. The mode shape have also been compared with the results obtained in COMSOL and show satisfactory agreement.

In conclusion, the proposed method can improve the computation efficiency for computing the dispersion relations of lattice structures dramatically and it ensures no natural frequency is missed in the whole frequency range. The method presented can be applied for the wave propagation analysis and design of complex lattice structures.

### Declaration of competing interest

The authors declare that they have no known competing financial interests or personal relationships that could have appeared to influence the work reported in this paper.

### Acknowledgments

The authors appreciate the supports from National Natural Science Foundation (Grant Nos. 11802345), State Key Laboratory of High Performance Complex Manufacturing (Grant No. ZZYJKT2019-07), Initial Funding of Specially-appointed Professorship (Grant No. 502045001) which made this research possible.

### References

- [1] M.S. Anderson, Vibration of prestressed periodic lattice structures, *AIAA J.* 20 (4) (1982) 551–555, <http://dx.doi.org/10.2514/3.51107>.
- [2] W.E. Lee, *Cellular solids, structure and properties*, *Mater. Sci. Technol.* 16 (2) (2000) 233.
- [3] D.H. Chen, S. Ozaki, Analysis of in-plane elastic modulus for a hexagonal honeycomb core : Effect of core height and proposed analytical method, *Compos. Struct.* 88 (1) (2009) 17–25, <http://dx.doi.org/10.1016/j.compstruct.2008.02.021>.
- [4] M. Ruzzene, F. Scarpa, Directional and band-gap behavior of periodic auxetic lattices, *Phys. Status Solidi b* 680 (3) (2005) 665–680, <http://dx.doi.org/10.1002/pssb.200460385>.
- [5] S. Sepehri, H. Jafari, M.M. Mashhadi, M.R.H. Yazdi, M.M.S. Fakhrabadi, Study of tunable locally resonant metamaterials: Effects of spider-web and snowflake hierarchies, *Int. J. Solids Struct.* 204–205 (2020) 81–95, <http://dx.doi.org/10.1016/j.ijsolstr.2020.08.014>.
- [6] Z. Zhang, T. Li, Z. Wang, Y. Tang, Band gap characteristics of flexural wave of two-dimensional periodic frame structure composed of locally resonant composite beam, *Mech. Syst. Signal Process.* 131 (2019) 364–380, <http://dx.doi.org/10.1016/j.ymsp.2019.05.060>.
- [7] M. Li, S. Du, F. Li, X. Jing, Vibration characteristics of novel multilayer sandwich beams: Modelling, analysis and experimental validations, *Mech. Syst. Signal Process.* 142 (2020) 106799, <http://dx.doi.org/10.1016/j.ymsp.2020.106799>.
- [8] S. Timorian, M. Ouisse, N. Bouhaddi, S. De Rosa, F. Franco, Numerical investigations and experimental measurements on the structural dynamic behaviour of quasi-periodic meta-materials, *Mech. Syst. Signal Process.* 136 (2020) 106516, <http://dx.doi.org/10.1016/j.ymsp.2019.106516>.
- [9] J. Meng, Z. Deng, K. Zhang, X. Xu, Wen, Band gap analysis of star-shaped honeycombs with varied Poissons ratio, *Smart Mater. Struct.* (2015) <http://dx.doi.org/10.1088/0964-1726/24/9/095011>.
- [10] E.J.P. Miranda, J.M.C.D. Santos, Evanescent Bloch waves and complex band structure in magnetoelectroelastic phononic crystals, *Mech. Syst. Signal Process.* 112 (2018) 280–304, <http://dx.doi.org/10.1016/j.ymsp.2018.04.034>.
- [11] D. Yu, Y. Liu, J. Qiu, G. Wang, H. Zhao, Complete flexural vibration band gaps in membrane-like lattice structures, *Phys. Lett. A* 357 (2006) 154–158, <http://dx.doi.org/10.1016/j.physleta.2006.04.034>.
- [12] A. Bacigalupo, L. Gambarotta, Simplified modelling of chiral lattice materials with local resonators, *Int. J. Solids Struct.* 83 (2016) 126–141, <http://dx.doi.org/10.1016/j.ijsolstr.2016.01.005>.
- [13] K. Zhang, P. Zhao, C. Zhao, F. Hong, Z. Deng, Study on the mechanism of band gap and directional wave propagation of the auxetic chiral lattices, *Compos. Struct.* 238 (January) (2020) <http://dx.doi.org/10.1016/j.compstruct.2020.111952>.
- [14] D. Qi, H. Yu, W. Hu, C. He, W. Wu, Bandgap and wave attenuation mechanisms of innovative reentrant and anti-chiral hybrid auxetic metastructure, *Extrem. Mech. Lett.* 28 (2019) 58–68, <http://dx.doi.org/10.1016/j.eml.2019.02.005>.
- [15] S. Mukherjee, F. Scarpa, S. Gopalakrishnan, Phononic band gap design in honeycomb lattice with combinations of auxetic and conventional core, *Smart Mater. Struct.* (2016).
- [16] X. Wang, T.J. Lu, Optimized acoustic properties of cellular solids, *J. Acoust. Soc. Am.* 106 (December 1998) (2014) 756–765, <http://dx.doi.org/10.1121/1.427094>.
- [17] A.G. Evans, A.G. Evans, P. Materials, Lightweight materials and structures, *MRS Bull.* (October) (2001) 790–797, <http://dx.doi.org/10.1557/mrs2001.206>.
- [18] T. Kim, H.P. Hodson, T.J. Lu, Fluid-flow and endwall heat-transfer characteristics of an ultralight lattice-frame material, *Int. J. Heat Mass Transfer* 47 (6–7) (2004) 1129–1140, <http://dx.doi.org/10.1016/j.ijheatmasstransfer.2003.10.012>.
- [19] T. Mukhopadhyay, S. Adhikari, Stochastic mechanics of metamaterials, *Compos. Struct.* 162 (2016) 85–97, <http://dx.doi.org/10.1016/j.compstruct.2016.11.080>.
- [20] Y. Prawoto, Seeing auxetic materials from the mechanics point of view: A structural review on the negative Poisson's ratio, *Comput. Mater. Sci.* 58 (2012) 140–153, <http://dx.doi.org/10.1016/j.commatsci.2012.02.012>.
- [21] H.L. Fan, F.N. Jin, D.N. Fang, Mechanical properties of mer. Part I : Analysis, *Compos. Sci. Technol.* 68 (15–16) (2008) 3380–3387, <http://dx.doi.org/10.1016/j.compotech.2008.09.022>.
- [22] Y. Li, H. Li, Bandgap merging and widening of elastic metamaterial with heterogeneous, *J. Phys. D: Appl. Phys.* (2020) <http://dx.doi.org/10.1088/1361-6463/abab2b>.
- [23] K. Wang, J. Zhou, D. Xu, H. Ouyang, Lower band gaps of longitudinal wave in a one-dimensional periodic rod by exploiting geometrical nonlinearity, *Mech. Syst. Signal Process.* 124 (2019) 664–678, <http://dx.doi.org/10.1016/j.ymsp.2019.02.008>.
- [24] Z. Wu, W. Liu, F. Li, C. Zhang, Band-gap property of a novel elastic metamaterial beam with X-shaped local resonators, *Mech. Syst. Signal Process.* 134 (2019) 106357, <http://dx.doi.org/10.1016/j.ymsp.2019.106357>.
- [25] L. Rayleigh, XVII. On the maintenance of vibrations by forces of double frequency, and on the propagation of waves through a medium endowed with a periodic structure, *Lond. Edinb. Dublin Philos. Mag. J. Sci.* 24 (147) (1887) <http://dx.doi.org/10.1080/14786448708628074>.

- [26] L. Brillouin, *Wave propagation in periodic structures: electric filters and crystal lattices*, 1953.
- [27] D.J. Mead, Wave propagation in continuous periodic structures : Research contributions from southampton, *J. Sound Vib.* 190 (1996) 495–524, <http://dx.doi.org/10.1006/jsvi.1996.0076>.
- [28] D.J. Mead, A general theory of harmonic wave propagation in linear periodic systems with multiple coupling, *J. Sound Vib.* 27 (1973) 235–260, [http://dx.doi.org/10.1016/0022-460X\(73\)90064-3](http://dx.doi.org/10.1016/0022-460X(73)90064-3).
- [29] D.J. Mead, *Wave propagation and natural modes in periodic systems: II. Multi-coupled systems, with and without damping*, *J. Sound Vib.* 40 (1975) 19–39.
- [30] S. Gonnella, M.R. Á, Analysis of in-plane wave propagation in hexagonal and re-entrant lattices, *J. Sound Vib.* 312 (2008) 125–139, <http://dx.doi.org/10.1016/j.jsv.2007.10.033>.
- [31] A. Martinsson, P.G. Movchan, Vibrations of lattice structures and phononic band gaps, *Quart. J. Mech. Appl. Math.* 56 (2003) (2002) 45–64, <http://dx.doi.org/10.1093/qjmam/56.1.45>.
- [32] F. Casadei, J.J. Rimoli, Anisotropy-induced broadband stress wave steering in periodic lattices, *Int. J. Solids Struct.* 50 (9) (2013) 1402–1414, <http://dx.doi.org/10.1016/j.ijsolstr.2013.01.015>.
- [33] A.S. Phani, J. Woodhouse, N.A. Fleck, Wave propagation in two-dimensional periodic lattices, *J. Acoust. Soc. Am.* (2006) <http://dx.doi.org/10.1121/1.2179748>.
- [34] C.W. Zhou, X.K. Sun, J.P. Laine, M.N. Ichchou, A. Zine, S. Hans, C. Boutin, Wave propagation feature in two-dimensional periodic beam lattice with local resonance by numerical method and analytical homogenization approach, *Int. J. Mech.* (2018) <http://dx.doi.org/10.1142/S1758825118500424>.
- [35] E.D. Nobrega, F. Gautier, A. Pelat, J.M.C.D. Santos, Vibration band gaps for elastic metamaterial rods using wave finite element method, *Mech. Syst. Signal Process.* 79 (2016) 192–202, <http://dx.doi.org/10.1016/j.ymsp.2016.02.059>.
- [36] J. Mencik, D. Duhamel, A wave-based model reduction technique for the description of the dynamic behavior of periodic structures involving arbitrary-shaped substructures and large-sized finite element models, *Finite Elem. Anal. Des.* 101 (2015) 1–14, <http://dx.doi.org/10.1016/j.finel.2015.03.003>.
- [37] E.B. Chin, A.A. Mokhtari, A. Srivastava, N. Sukumar, Spectral extended finite element method for band structure calculations in phononic crystals, *J. Comput. Phys.* 427 (2021) 110066, <http://dx.doi.org/10.1016/j.jcp.2020.110066>.
- [38] T. Chen, L. Wang, Suppression of bending waves in a periodic beam with timoshenko beam theory, *Acta Mech. Solida Sin.* 26 (2) (2013) 177–188, [http://dx.doi.org/10.1016/S0894-9166\(13\)60017-8](http://dx.doi.org/10.1016/S0894-9166(13)60017-8).
- [39] A.A. Kutsenko, A.J. Nagy, X. Su, A.L. Shuvalov, A.N. Norris, Wave propagation and homogenization in 2d and 3d lattices: A semi-analytical approach, *Quart. J. Mech. Appl. Math.* 70 (2) (2017) 131–151, <http://dx.doi.org/10.1093/qjmam/hbx002>.
- [40] M.J. Leamy, Exact wave-based Bloch analysis procedure for investigating wave propagation in two-dimensional periodic lattices, *J. Sound Vib.* 331 (7) (2012) 1580–1596, <http://dx.doi.org/10.1016/j.jsv.2011.11.023>.
- [41] S. Adhikari, T. Mukhopadhyay, X. Liu, Broadband dynamic elastic moduli of honeycomb lattice materials: A generalized analytical approach, *Mech. Mater.* 157 (2021) 103796, <http://dx.doi.org/10.1016/j.mechmat.2021.103796>.
- [42] X. Liu, C. Sun, J. Ranjan Banerjee, H.-C. Dan, L. Chang, An exact dynamic stiffness method for multibody systems consisting of beams and rigid-bodies, *Mech. Syst. Signal Process.* 150 (107264) (2021) <http://dx.doi.org/10.1016/j.ymsp.2020.107264>.
- [43] X. Liu, Y. Li, Y. Lin, J.R. Banerjee, Spectral dynamic stiffness theory for free vibration analysis of plate structures stiffened by beams with arbitrary cross-sections, *Thin-Walled Struct.* 160 (2021) 107391, <http://dx.doi.org/10.1016/j.tws.2020.107391>.
- [44] P. Xiang, Q. Xia, L.Z. Jiang, L. Peng, J.W. Yan, X. Liu, Free vibration analysis of FG-CNTRC conical shell panels using the kernel particle ritz element-free method, *Compos. Struct.* 255 (2021) 112987, <http://dx.doi.org/10.1016/j.compstruct.2020.112987>.
- [45] X. Liu, X. Liu, W. Zhou, An analytical spectral stiffness method for buckling of rectangular plates on Winkler foundation subject to general boundary conditions, *Appl. Math. Model.* 86 (2020) 36–53, <http://dx.doi.org/10.1016/j.apm.2020.05.010>.
- [46] X. Liu, X. Liu, S. Xie, A highly accurate analytical spectral flexibility formulation for buckling and wrinkling of orthotropic rectangular plates, *Int. J. Mech. Sci.* 168 (2020) 105311, <http://dx.doi.org/10.1016/j.ijmecsci.2019.105311>.
- [47] X. Liu, J.R. Banerjee, Free vibration analysis for plates with arbitrary boundary conditions using a novel spectral-dynamic stiffness method, *Comput. Struct.* 164 (2016) 108–126, <http://dx.doi.org/10.1016/j.compstruc.2015.11.005>.
- [48] X. Liu, L. Chang, J.R. Banerjee, H.-C. Dan, Closed-form dynamic stiffness formulation for exact modal analysis of tapered and functionally graded beams and their assemblies, *Int. J. Mech. Sci.* 214 (2022) 106887, <http://dx.doi.org/10.1016/j.ijmecsci.2021.106887>.
- [49] X. Liu, X. Liu, S. Adhikari, S. Yin, Extended witztrick-williams algorithm for eigenvalue solution of stochastic dynamic stiffness method, *Mech. Syst. Signal Process.* 166 (2022) 108354, <http://dx.doi.org/10.1016/j.ymsp.2021.108354>.
- [50] X. Liu, S. Qiu, S. Xie, J.R. Banerjee, Extension of the Witztrick-Williams algorithm for free vibration analysis of hybrid dynamic stiffness models connecting line and point nodes, *Math.* 10 (1) (2022) <http://dx.doi.org/10.3390/math10010057>.
- [51] J.R. Banerjee, Review of the dynamic stiffness method for free-vibration analysis of beams, *Transp. Saf. Environ.* 1 (2) (2019) 106–116, <http://dx.doi.org/10.1093/tse/tdz005>.
- [52] J.R. Banerjee, F.W. Williams, An exact dynamic stiffness matrix for coupled extensional-torsional vibration of structural members, *Comput. Struct.* 50 (2) (1994) 161–166, [http://dx.doi.org/10.1016/0045-7949\(94\)90292-5](http://dx.doi.org/10.1016/0045-7949(94)90292-5).
- [53] J.R. Banerjee, Development of an exact dynamic stiffness matrix for free vibration analysis of a twisted timoshenko beam, *J. Sound Vib.* 270 (1) (2004) 379–401, [http://dx.doi.org/10.1016/S0022-460X\(03\)00633-3](http://dx.doi.org/10.1016/S0022-460X(03)00633-3).
- [54] M. Ruzzene, F. Scarpa, F. Soranna, Wave beaming effects in two-dimensional cellular structures, *Smart Mater. Struct.* 12 (2003) 363–372, <http://dx.doi.org/10.1088/0964-1726/12/3/307>.
- [55] J.R. Banerjee, S.O. Papkov, X. Liu, D. Kennedy, Dynamic stiffness matrix of a rectangular plate for the general case, *J. Sound Vib.* 342 (2015) 177–199, <http://dx.doi.org/10.1016/j.jsv.2014.12.031>.
- [56] S. Zuo, F. Li, C. Zhang, Numerical and experimental investigations on the vibration band-gap properties of periodic rigid frame structures, *Acta Mech. Sinica* 1669 (2016) 1653–1669, <http://dx.doi.org/10.1007/s00707-016-1587-4>.
- [57] Z. Wu, Y. Wang, F. Li, Analysis on band gap properties of periodic structures of bar system using the spectral element method, *Waves Random Complex Media* 5030 (2013) 349–372, <http://dx.doi.org/10.1080/17455030.2013.830798>.
- [58] F. Gao, Z. Wu, F. Li, C. Zhang, Numerical and experimental analysis of the vibration and band-gap properties of elastic beams with periodically variable cross sections, *Waves Random Complex Media* 5030 (2019) 1–18, <http://dx.doi.org/10.1080/17455030.2018.1430918>.
- [59] Z. Wu, F. Li, Spectral element method and its application in analysing the vibration band gap properties of two-dimensional square lattices, *J. Vib. Control* (October 2013) (2014) <http://dx.doi.org/10.1177/1077546314531805>.
- [60] Z. Wu, F. Li, C. Zhang, Vibration band-gap properties of three-dimensional kagome lattices using the spectral element method, *J. Sound Vib.* 341 (2015) 162–173, <http://dx.doi.org/10.1016/j.jsv.2014.12.038>.
- [61] X. An, H. Fan, C. Zhang, Elastic wave and vibration bandgaps in planar square metamaterial-based lattice structures, *J. Sound Vib.* 475 (2020) <http://dx.doi.org/10.1016/j.jsv.2020.115292>.
- [62] W. Wittrick, F. Williams, A general algorithm for computing natural frequencies of elastic structures, *Quart. J. Mech. Appl. Math.* 24 (3) (1971) 263–284, <http://dx.doi.org/10.1093/qjmam/24.3.263>.

- [63] X. Sun, The application of the wittick–williams algorithm for free vibration analysis of cracked skeletal structures, *Thin-Walled Struct.* 159 (2021) 107307, <http://dx.doi.org/10.1016/j.tws.2020.107307>.
- [64] X. Chen, K. Ye, An exact dynamic stiffness formulation for predicting natural frequencies of moderately thick shells of revolution, *Math. Probl. Eng.* 2018 (2018) <http://dx.doi.org/10.1155/2018/4156360>.
- [65] F.W. Williams, W.X. Zhong, P.N. Bennett, Computation of the eigenvalues of wave propagation in periodic substructural systems, *J. Vib. Acoust.* 115 (October 1993) (2017) 422–426, <http://dx.doi.org/10.1115/1.2930367>.
- [66] W.X. Zhong, F.W. Williams, On the direct solution of wave propagation for repetitive structures, *J. Sound Vib.* 181 (1995) 485–501.
- [67] M. Zhou, W. Zhong, F.W. Williams, Wave propagation in substructural chain-type structures excited by harmonic forces, *Int. J. Mech. Sci.* 35 (11) (1993) 953–964, [http://dx.doi.org/10.1016/0020-7403\(93\)90032-P](http://dx.doi.org/10.1016/0020-7403(93)90032-P).
- [68] W.X. Zhong, F.W. Williams, A.Y.T. Leung, Symplectic analysis for periodical electro-magnetic waveguides, *J. Sound Vib.* 267 (2003) 227–244, [http://dx.doi.org/10.1016/S0022-460X\(02\)01451-7](http://dx.doi.org/10.1016/S0022-460X(02)01451-7).
- [69] X.-H. Hou, Z.-C. Deng, J. Zhou, T.-Q. Liu, Symplectic analysis for elastic wave propagation in two-dimensional cellular structures, *Acta Mech. Sinica* 26 (2010) 711–720, <http://dx.doi.org/10.1007/s10409-010-0373-0>.
- [70] T. Bridges, Multi-symplectic structures and wave propagation, *Math. Proc. Cambridge Philos. Soc.* 121 (1997) 147–190, <http://dx.doi.org/10.1017/S0305004196001429>.
- [71] W. Hu, Z. Deng, S. Han, W. Zhang, Generalized multi-symplectic integrators for a class of Hamiltonian nonlinear wave PDEs, *J. Comput. Phys.* 235 (2013) 394–406, <http://dx.doi.org/10.1016/j.jcp.2012.10.032>.
- [72] W. Hu, Z. Wang, Y. Zhao, Z. Deng, Symmetry breaking of infinite-dimensional dynamic system, *Appl. Math. Lett.* 103 (2020) 106207, <http://dx.doi.org/10.1016/j.aml.2019.106207>.
- [73] W. Hu, C. Zhang, Z. Deng, Vibration and elastic wave propagation in spatial flexible damping panel attached to four special springs, *Commun. Nonlinear Sci. Numer. Simul.* 84 (2020) 105199, <http://dx.doi.org/10.1016/j.cnsns.2020.105199>.
- [74] W. Hu, J. Ye, Z. Deng, Internal resonance of a flexible beam in a spatial tethered system, *J. Sound Vib.* 475 (2020) 115286, <http://dx.doi.org/10.1016/j.jsv.2020.115286>.
- [75] W. Hu, M. Xu, J. Song, Q. Gao, Z. Deng, Coupling dynamic behaviors of flexible stretching hub-beam system, *Mech. Syst. Signal Process.* 151 (2021) 107389, <http://dx.doi.org/10.1016/j.ymsp.2020.107389>.
- [76] W. Hu, Y. Huai, M. Xu, X. Feng, R. Jiang, Y. Zheng, Z. Deng, Mechano-electrical flexible hub-beam model of ionic-type solvent-free nanofluids, *Mech. Syst. Signal Process.* 159 (2021) 107833, <http://dx.doi.org/10.1016/j.ymsp.2021.107833>.
- [77] J. Meng, Z. Deng, K. Zhang, X. Xu, Wave propagation in hexagonal and re-entrant lattice structures with cell walls of non-uniform thickness, *Waves Random Complex Media* (2015) 37–41, <http://dx.doi.org/10.1080/17455030.2015.1005195>.
- [78] Y. Mochida, S. Ilanko, On the Rayleigh-Ritz method, Gorman's superposition method and the exact dynamic stiffness method for vibration and stability analysis of continuous systems, *Thin-Walled Struct.* 161 (2021) 107470, <http://dx.doi.org/10.1016/j.tws.2021.107470>.
- [79] L. Cremer, H.O. Leilich, Zur theorie der biegekettenteiler, *Arch. Der Elektrischen Übertragung* 7 (1953) 261–270.
- [80] M.J. Leamy, Analysis of Bloch's method and the propagation technique in periodic structures, *J. Vib. Acoust.* 133 (2016) 1–7, <http://dx.doi.org/10.1115/1.4003202>.
- [81] X. Liu, Y. Zhao, W. Zhou, J.R. Banerjee, Dynamic stiffness method for exact longitudinal free vibration of rods and trusses using simple and advanced theories, *Appl. Math. Model.* 104 (2022) 401–420, <http://dx.doi.org/10.1016/j.apm.2021.11.023>.
- [82] J.R. Banerjee, A. Ananthapuvirajah, An exact dynamic stiffness matrix for a beam incorporating Rayleigh–Love and Timoshenko theories, *Int. J. Mech. Sci.* 150 (2019) 337–347, <http://dx.doi.org/10.1016/j.ijmecsci.2018.10.012>.
- [83] D. Karli, M. Caji, T. Chatterjee, S. Adhikari, Wave propagation in mass embedded and pre-stressed hexagonal lattices, *Compos. Struct.* 256 (July 2020) (2021) <http://dx.doi.org/10.1016/j.compstruct.2020.113087>.